Scheme for optimising the power of an induction motor utilising FLC in an electric vehicle

1)GANDHAM UDAY KIRAN , 2)BHAGYASHREE BEHARA ,3)TELU LAKSHMI NARAYANA , 4)DANDA KARTHIK , 5)RONGALA HEMA VENKATA VANAJA, 6)KASARAPU SATHISH KUMAR

1.Student, Electrical and Electrical Engineering , Sanketika vidhya parishad engineering college, Visakhapatnam, Andhra Pradesh

2 Student, Electrical and Electrical Engineering , Sanketika vidhya parishad engineering college, Visakhapatnam, Andhra Pradesh

3 Student, Electrical and Electrical Engineering , Sanketika vidhya parishad engineering college, Visakhapatnam, Andhra Pradesh

4 Student, Electrical and Electrical Engineering , Sanketika vidhya parishad engineering college, Visakhapatnam, Andhra Pradesh

5 Student, Electrical and Electrical Engineering , Sanketika vidhya parishad engineering college, Visakhapatnam, Andhra Pradesh

6 Assistant Professor , Electrical and Electrical Engineering , Sanketika vidhya parishad engineering college, Visakhapatnam, Andhra Pradesh

ABSTRACT

Energy efficiency is crucial in electric and hybrid vehicles (EVs) since their energy storage capacity is restricted. In addition to its great stability and inexpensive cost, loss minimization increases the induction motor's efficiency. Additionally, while it is functioning at a load lower than maximum, it may use more power than is necessary to do its task. This research suggests a fuzzy logic control (FLC)-based approach for electric vehicle applications. The FLC controller can conserve more power and enhance the amplitude of the beginning current. The MATLAB/SIMULINK software programme was utilised to verify the control's performance through simulation. The simulation schemes demonstrate rapid rejection of disturbances affecting the system and good, high-performance outcomes in the time-domain response when compared to the traditional proportional integral derivative controller. As a result, the induction motor's core losses are significantly decreased, increasing the driving system's efficiency.

1 Introduction

The substantial increase in fossil fuel consumption, especially in the previous several decades, has resulted in a rise in CO2 concentration within the atmosphere. As a result of growing concerns about climate change and sea level rise brought on by global warming, there is an urgent need for worldwide initiatives to cut carbon dioxide. Vehicle fuel efficiency needs to be significantly increased because transportation contributes roughly 20% of all carbon dioxide emissions [1-6]. Because they are quieter, more ecologically friendly, more efficient, and typically less dependent on fuel, electric vehicles (EVs) have several benefits [7]. The cost and efficiency of the drive are significantly impacted by the selection of the electric machine. Electric motors, on the other hand, are a necessary component of every drive, including hybrid and EV models [8]. Induction and synchronous motors the primary machine types that can be used in electric vehicles (EVs) are motors (IMs) [9]. The following propulsion should be included in the EV-drive motor [7, 10–12]:

(I) high efficiency to extend driving distance; (ii) high torque density to provide sufficient driving force during starter, climbing, and accelerating;

(iii) the ability to regulate flow well enough to increase the range of static power speeds.

Because of its robustness, low cost, and low maintenance requirements, the IM is the ideal option for EVs and is more frequently used for the traction drive [13–16], although its losses are much larger in the EV application [17, 18], which causes the machine's efficiency to decline. The main obstacles to incorporating these vehicles into the transportation system are their increased weight, low energy density, extended battery life, and longer charging periods [19]. Therefore, the efficient utilisation of energy is essential to the functioning of electric vehicles [20–22]. It is widely accepted that proportional integral derivative (PID) control, which is utilised in many industrial

drives, is one of the most shared parts. Moreover, PID controllers are employed in industrial applications and are a part of most control loops currently in use [23, 24]. Significant performance deterioration may happen when operating conditions are changed because components may become obsolete or the working environment may change [25]. Fuzzy logic control (FLC) is one intelligent control technique that can deliver better performance than accurate analytical modelling of a controlled system since it is less uncertain and easier to use [26–28].

Numerous strategy rules that employ linguistic tags more simply are provided by the FLC framework. Numerous other studies on energy demand control in EVs have employed this strategy [7]. FLC is a model-free manner, it is not dependent on a controlled system mathematical model [28, 29]. Therefore, the FLC system controller should be built with adaptive qualities when the system reaches areas with fixed mistakes to improve the performance of the EV traction. Other themes in FLC include finding appropriate trade-offs between minimum overshoot, minimum steady-state error, and quick ascending time [30].

Nonetheless, the goal of the current design approaches is to lower steady-state losses [31, 32]. During transportation, the machine may have high and excessive current peak losses with variable flow linkages in cases where high stability efficiency is the design goal for traditional induction machines. As a result, the losses of transient machines that happen during the extremely dynamic driving cycle that the EV traction motor drive often experiences are the main topic of this article.

Numerous alternative control structures for EV applications have been presented in the literature. Among these are straightforward linear methods like direct torque and field-oriented control [8, 33], sliding mode control [36] and control [34, 35]. Lower secondary winding harmonic losses with the finite element approach [17], utilising the golden section method [33], a model reference adaptive system with an optimum base power scheme. Using the adaptive quadratic interpolation-based search controller (SC) to maximise the loss of the IM drive [20] and the fuzzy controller with nine rules for slip control, which produces frequency by using the change in speed error as an input.

For EV applications, an FLC-based approach is suggested in this paper. Next, a comparison of the controllers (PID and FLC) is shown according to how they affect IM execution. The primary outputs from this work are

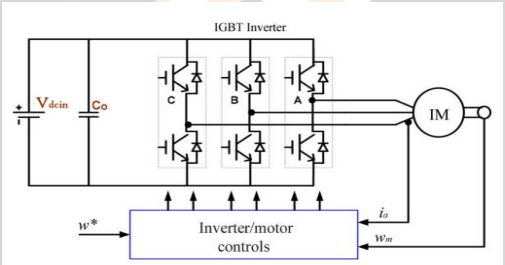

Fig. 1 EV drive with an IM

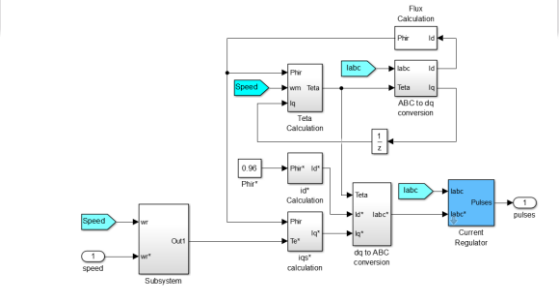

Fig. 2 Control system of IM

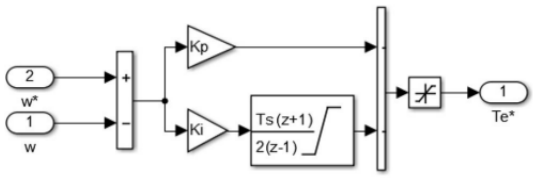

Fig. 3 Block diagram of the conventional PID controller

be summed up like this: Efficiency is a measure of energy cost, and the primary goal is to reduce the cost of the drive life cycle at projected speeds and higher. The inverter's efficiency depends on the overall driving efficiency.

The remainder of the document is structured as follows: The circuit description is provided in Section 2, and the control theory is stated in Section 3. In Section 4, the efficiency of the IM drive and power loss calculations are examined. The simulation results are shown in Section 5, the experimental results are conducted and reported in Section 6, and the conclusion is provided in Section 7.

2 Circuit description

As seen in Fig. 1, a battery-electric vehicle (BEV) is an electrically powered vehicle that is composed of three basic components: an electric motor system, which is often a single electrical machine (commonly a three phase AC). connected to the wheel through the differential and gearbox. Secondly, there is a battery that stores energy chemically. The battery is connected to the gadget by an electronic DC/AC power adapter along with the control system. The electric machine is finally equipped with a three-phase frequency and voltage control system that adjusts its operation according on the demands of the driver. This system is coupled to the accelerator and/or brake pedals.

The three-phase electric machine in Fig. 1 powers the wheels' traction. The electric motor shaft's high-speed adjustment to the low speed of the differential with a gear ratio. The left and right wheels will be powered by the wheels. An inverter, which changes the DC battery electricity to three-phase AC voltage, regulates the machine's speed. When assessing the power consumption of an electric vehicle (EV) that is not connected to the grid, it is crucial to account for component losses. Our promise is to develop appropriate controllers for feedback to force the EV system into the necessary functionality. Using FLC approaches, the insufficiently powerful, flexible, and adaptive controller may be put into practice for EVs applications.

3 Control principle

3.1 Conventional PID control

In the first design method, a traditional PID controller is used to control the speed of an indirect field-oriented IM order. Additionally, the starting situation is examined. As demonstrated. A phase-locked loop algorithm that synchronises with the utility current regulator and (direct-quadrature-zero) conversion equations are included in the proposed control system shown in Fig. 2. The phase currents (ia, ib, and ic) are transformed into a d–q frame from a–b–c coordinates. The following conversions can be used to characterise the elements of d–q:

$$\begin{bmatrix} i_d \\ i_q \end{bmatrix} = \sqrt{\frac{2}{3}} \begin{bmatrix} \sin(\omega t) & \sin\left(\omega t - \frac{2\pi}{3}\right) & \sin\left(\omega t + \frac{2\pi}{3}\right) \\ \cos(\omega t) & \cos\left(\omega t - \frac{2\pi}{3}\right) & \cos\left(\omega t + \frac{2\pi}{3}\right) \end{bmatrix} \times \begin{bmatrix} i_{sa} \\ i_{sb} \\ i_{sc} \end{bmatrix} \quad (1)$$

Average and oscillation components are now included in the computation of active and reactive power. To obtain the average components to the outputs of the PID control loops, however, two external PID control loops are used both reactive and active power. Fig. 3 shows a block diagram of the traditional PID control. According to the following conversions, this PID generates active current reference (id*) and reactive current reference (iq*):

$$i_d^* = k_p(P_{ref} - P) + k_i \int (P_{ref} - P)\, dt \quad (2)$$

$$i_q^* = k_p(Q_{ref} - Q) + k_i \int (Q_{ref} - Q)\, dt \quad (3)$$

If ki is the basic constant and kp is the proportional constant, for the employed PID controllers. The charging power reference is called Pref, and the reactive power needed by the AC source is called Qref.

The inner current loop and the outer voltage loop are integrated to provide the control. The current is produced in the outer loop when the real current and the current reference are compared reference, and the inner loop is managed by it. As a result, by comparing the measured line currents acquired via the park conversion, the internal PID loops are produced. To obtain the operating ratios in the d–q coordinates, the findings (ed and eq) are first summed by the disengagement conditions and then normalised by the DC voltage as follows:

$$\begin{bmatrix} d_d \\ d_q \end{bmatrix} = \frac{1}{V_{\mathrm{dc}}} \begin{bmatrix} e_d + v_d + 3\omega L \times i_q \\ e_q + v_q - 3\omega L \times i_d \end{bmatrix} \quad (4)$$

The duty ratios in (a, b, and c) frame coordinates can be obtained by inverse matrix transformation and are represented as follows:

$$\begin{bmatrix} D_a \\ D_b \\ D_c \end{bmatrix} = \sqrt{\frac{2}{3}} \begin{bmatrix} \sin(\omega t) & \cos(\omega t) \\ \sin\left(\omega t - \frac{2\pi}{3}\right) & \cos\left(\omega t - \frac{2\pi}{3}\right) \\ \sin\left(\omega t + \frac{2\pi}{3}\right) & \cos\left(\omega t + \frac{2\pi}{3}\right) \end{bmatrix} \times \begin{bmatrix} d_d \\ d_q \end{bmatrix} \quad (5)$$

3.2 Description of suggested FLC

Controlling this issue continues to be challenging due to the non-linear characteristics of AC motors, particularly the squirrel cage induction motor (SCIM), since numerous parameters (primarily rotor resistances) change depending on the operational environment. Consequently, for EV applications, the effective intelligent FLC [37] must be used to modify the conventional control technology (PID). When designing a fuzzy system, the most crucial variables to consider are:

(i) the development of fuzzy rules by subject matter experts for specific control challenges;
(ii) (ii) the selection and adjustment of membership functions; and
(iii) the selection of scaling factors.

The basic FLC for EV applications was created using the second design technique. EV applications are a well-established application for variable structure control units that are known for their stability and longevity. Figure 4 depicts a standard FLC.

Fuzzy logic is a mathematical technique that provides improved voltage, frequency, and current control for adjustable speed drives. It can be used in EV applications to solve issues when non-linearity and its dynamic nature are too difficult for traditional control techniques to handle. These kinds of issues are all present in motor control.

3.3 Speed control using FLC

In the case of motor speed control, FLC requires two input variables: the motor speed error (we) and its derivative, which stands for the speed variation error (Δwe). Speed and mistake of speed. One way to explain variation error would be as follows:

$$we = w^{*}_{\mathrm{ref}} - w_{\mathrm{act}} \quad (6)$$

where the terms "w*ref" and "wact" stand for the actual/measured motor speed and the reference motor speed, respectively:

$$\frac{\mathrm{d}we}{\mathrm{d}t} = \frac{\Delta we}{T_s} \quad (7)$$

The incremental change in the control signal Δu is the controller output. It is possible to obtain the control signal by

$$\Delta u = \Delta t_e^* = k_1 \cdot we + k_2 \cdot \Delta we \quad (8)$$

where k1 and k2 stand for the former and present states of the system, in turn. As illustrated in Fig. 5, the normalised domain [−1, 1] defines the universe of discourse in all membership functions of the controller inputs, i.e., we and Δwe, and the output, i.e. Δu.

Fuzzy logic membership functions have been partitioned using five membership functions (MF) for inputs and five MF for output fuzzy sets, as seen in Figure 5.

In this system, two input variables are related to one output variable using a Mamdani fuzzy inference method. The error (we), which are the variations between the two input variables. The recorded speed, the desired speed (set-point), and the error change (Δwe). In Fig. 4, the scaling factors Ge, Gde, and Gu carry out the normalisation and denormalization of the individual variables of a traditional control gain. The value of these measurement factors is dependent on the starting error when Ge, Gde, and Gu stand for the error measurement, error variation, and FLC output factors, respectively. As illustrated in Fig. 5, limited models are employed to lower the error and variance in the error between (1, −1) the input and output functions of the FLC, while the FLC rules are

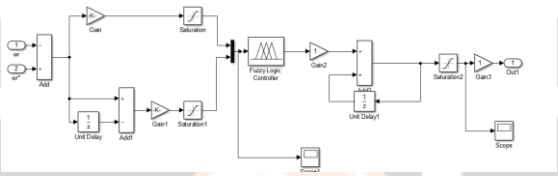

Fig. 4 Detailed construction of the fuzzy controller

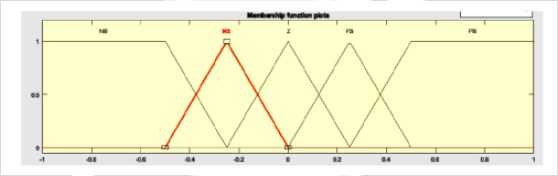

Fig. 5 Membership function of FLC (we), (Δwe), (Δu)

Table 1 Rules of the FLC

Δwe	we				
	NB	NS	Z	PS	PB
NB	NB	NB	NS	NS	Z
NS	NB	NS	NS	Z	PS
Z	NS	NS	Z	PS	PS
PS	NS	Z	PS	PS	PB
PB	Z	PS	PS	PB	PB

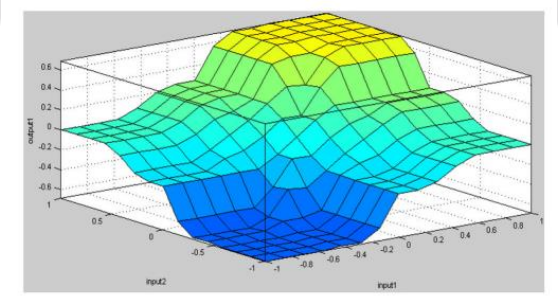

Fig. 6 Crisp in./out. Map

logged into Table 1. Rather of just taking NB, NS, Z, PS, and PB, this feature suggests that a more exact continuous control rule can be created by interpolating the basic table of rules represent, in that order, negative big, negative small, zero, positive small, and positive big. This time, symmetrical triangles with an equal base and 50% overlap with neighbouring MFs are picked, except for two obscure groups at the outer extremities (trapezoidal MFs are selected).

Each variable has five fuzzy subsets, as indicated in Table 1, providing a total of 25 potential rules. A common rule is "If e is NB and de is PB, then u is Z."

Because the perturbation approach modifies the motor speed and output power, speed correction control is required. The output rotor speed of the motor needs to be kept as steady as feasible.

Fig. 6 displays the input/output mapping for the FLC. By utilising this fuzzy controller in the outer loop and using the speed error and variation of error as input signals to build the equivalent control terms, smooth torque and improved system performance may be produced for EV applications.

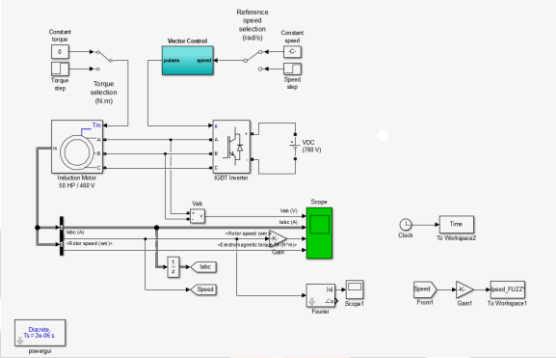

Fig. 8 MATLAB model of three-phase IM

4 Power loss calculations and efficiency of induction motor drive

To confirm the measured efficiency, the following power losses of the suggested control scheme are evaluated for a worst-case scenario at full load.

4.1 Parameters

The full set of supplied and computed parameters in Table 2 is displayed in this section. The datasheet's typical values are where the parameters originate. After then, a few computed parameters will be displayed. In [38], the stray losses are insignificant.

4.2 Input power losses

The three-phase inductive motor draws 60 A at 0.85 PF lagging with FLC and 62.6 A at 0.85 PF lagging with PID. It is possible to estimate the input power losses as

$$P_{\text{In}} = \sqrt{3} \times V_{\text{L}} I_{\text{L}} \cos\theta = 3 \times V_{\text{ph}} I_{\text{ph}} \cos\theta \quad (9)$$

4.3 Air-gap power losses

It is considered that the stator copper losses are 2 kW and the core losses are 1.8 kW. It is possible to estimate the air-gap power losses as

$$P_{\text{AG}} = P_{\text{In}} - (P_{\text{SCL}} + P_{\text{Core}})$$
$$= P_{\text{Conv}} + P_{\text{RCL}} = 3I_2^2 \frac{R_2}{S} = \frac{P_{\text{RCL}}}{S} \quad (10)$$

Table 2 Given and calculated parameters

Item	Symbol	Value
voltage (line-to-line)	V_L	460 V
frequency	F	60 Hz
number of poles	P	4
power factor	PF	0.85 lagging
three-phase IM is drawing (PID)	I_L	62.6 A
three-phase IM is drawing (FLC)	I_L	60 A
stator copper losses (PID)	P_{SCL}	2 kW
stator copper losses (FLC)	P_{SCL}	1.8 kW
rotor copper losses (PID)	P_{RCL}	700 W
rotor copper losses (FLC)	P_{RCL}	500 W
core losses	PC_{ore}	1.8 kW
friction and windage losses	$P_{F\&W}$	600 W

Table 3 Results of power losses analysis under full load and efficiency estimation of IM drive using PID and FLC

Item	Power losses calculation	PID	FLC
input power	$P_{In} = \sqrt{3} \times V_L I_L \cos\theta$ $= 3 \times V_{ph} I_{ph} \cos\theta$	42.395 kW	40.634 kW
air-gap power losses	$P_{AG} = P_{In} - (P_{SCL} + P_{Core})$	38.595 kW	37.034 kW
converted power losses	$P_{Conv} = P_{AG} - P_{RCL}$	37.895 kW	36.534 kW
output power	$P_{out} = P_{Conv} - (P_{f\&w} + P_{stray})$	37.295 kW	35.934 kW
efficiency	$\eta = \frac{P_{out}}{P_{in}} \times 100$	87.97%	88.43%

4.4 Converted power losses

The only rotor copper losses that are included in the power conversion calculation are 700 W. It is possible to estimate the converted power losses as

$$P_{Conv} = P_{AG} - P_{RCL} = 3I_2^2 \frac{R_2(1-S)}{S} = \frac{P_{RCL}(1-S)}{S} \quad (11)$$

$$P_{Conv} = (1-S)P_{AG} \quad (12)$$

4.5 Output power losses

The computation considers the assumption that stray losses are minimal, which means that the friction and windage losses are each 600 W. One way to evaluate the output power losses is as follows Table 3

$$P_{Out} = P_{Conv} - (P_{f+w} + P_{stray}) \quad (13)$$

The IM drive's efficiency in relation to load percentage is displayed in Fig. 7. According to this number, when the IM performs at its best, energy efficiency rises. By contrasting the outcomes obtained by the controller adjusted using a few well-known tuning rules and the outcomes produced by the recommended rules, the suggested method produces a more worthy performance.

5 Simulation results

Two examples have been examined in the simulation, which makes use of the MATLAB software's Simulink and power sum toolboxes, as seen in Fig. 8. The first case study uses a PID to power a 50-horsepower inline motor in charge. In the first five seconds of operation, three-phase voltage and current are recorded and planned.

The probe is also made in the torque that results from the acceleration curve. In the second scenario, FLC is used to run the motor directly. PID controller reaction is

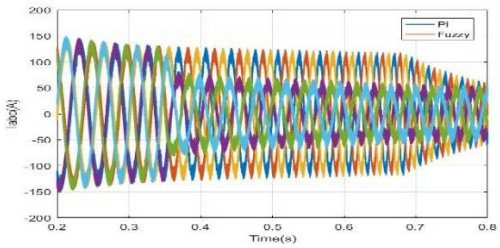

Fig. 9 Three-phase stator current of PID and FLC models (A)

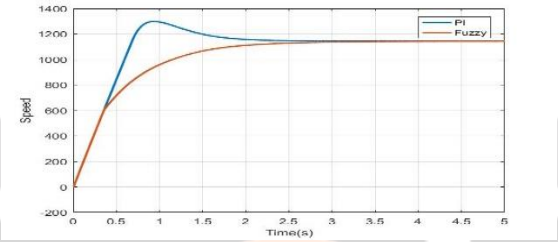

Fig. 10 Simulation response of PID and FLC for rotor speed (rpm)

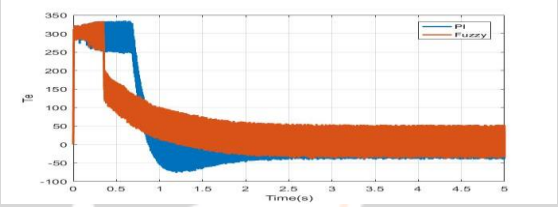

Fig. 11 Simulation response of PID and FLC for electromagnetic torque (N m)

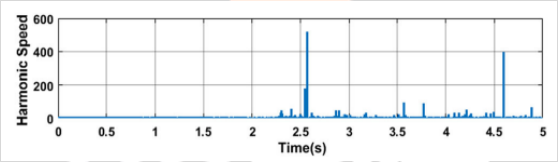

Fig. 12 Harmonic speed waveform of the PID model

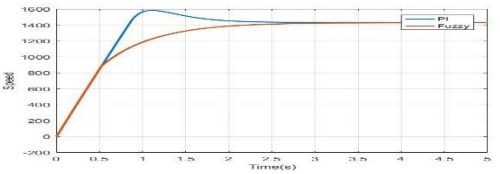

Fig. 14 Speed response comparison for PID and FLC when the reference speed is 1432 rpm

compared to the FLC reaction, with the outcomes displayed in Figs. 9–11.

Based on the provided data, with respect to the size of beginning currents, the temporal response of acceleration and its outputs have both improved. Less loss components in the same order of components are present in the phase current when using the recommended method. This demonstrates that the technique lowers the speed variation and produces an actual torque smoother [30]. The PID model is and the FLC model's harmonic speed waveforms are displayed in Figs. 12 and 13, respectively.

PID and FLC were both used in several simulation tests to regulate the IM speed. The speed reference was gradually changed at a to evaluate the control unit's performance results consistent torque at load, as depicted in Figs. 14–16. In terms of peak overshoot, settling time, and rising time, Table 4 compares the performance of FLC and PID when the multistep speed input is used. Table 4 makes it evident that FLC, when compared to PID

response for multistep speed input, offers a faster reaction in both settling and rising time, except for the rise time at 1145 (rpm). As a result, FLC performed better than PID. Furthermore, FLC demonstrated improved control over the three-phase IM's speed.

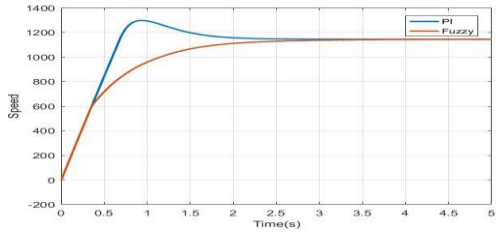

Fig. 15 Speed response comparison for PID and FLC when the reference speed is 1145 rpm

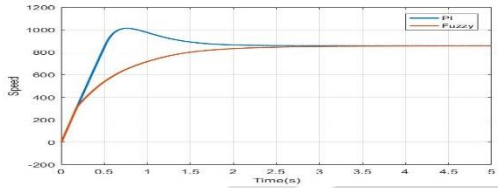

Fig. 16 Speed response comparison for PID and FLC when the reference speed is 859 rpm

give a quick, precise reaction that is largely free of overshoot and SteadyState inaccuracy.

PID and FLC were used in several simulation studies to manage the IM speed for EV applications. The simulations were conducted under a range of operational parameters, including applied load and reference speed. PID and FLC's respective performances were examined and contrasted. Figs. 17a and b illustrate the FLC's speed response for a range of reference speeds as well as how it performed during a load disturbance.

A 20-second simulation's findings are displayed in Fig. 18. The car comes to a complete stop at time t = 0 and the accelerator is abruptly depressed to 70%. Until there is power, the vehicle begins in electrical mode when the vehicle's need hits 10 kW (at t = 0.8 s). In t = 12 s, the brakes are applied to 70%. To transfer the brake energy to the battery and charge it for four seconds, this activates the electric motor. The accelerator is abruptly moved back to 70% at time t = 16 s [39].

Table 5 Circuit parameters

Item	Parameters	Symbol	Value	Unit
battery	DC input voltage	V_i	780	V
inverter	snubber resistance	R_s	1000	Ω
	forward voltages	V_f	0.8	V
	switching frequency	F_{SW}	10	kHz
IM	nominal power	P_n	37.3	kVA
	voltage (line–line)	V_L	460	Vrms
	frequency	F_n	60	Hz
	number of poles	P	4	—
	mutual inductance	L_m	34.7	mH
	stator resistance	R_s	0.087	Ω
	rotor resistance	R_r	0.228	Ω
	stator and rotor leakage inductance	$L_{ls} = L'_{lr}$	0.8	mH
	moment of inertia	J	1.662	kg m^2
	rated speed	N	1780	rpm
	friction coefficient	F_c	0.1	N m s
	rated power	P_o	50	hp

Table 6 Controller parameters

	$k_p/k_1/Ge$	$k_i/k_2/Gde$	$k_d/k_3/Gu$
PID	5	30	1
FLC	1/120	2500	1

controller. Additionally, the experimental findings agreed well with the simulated results.

Table 4 Comparison of FLC and PID performance in multistep speed response. The sampling time is Ts = 2e−6 s

Reference speed, rpm	Rise time, s		Settling time, s		Peak overshoot, %	
	FLC	PID	FLC	PID	FLC	PID
1432	0.731	0.681	1.982	2.584	0.501	10.55
1145	0.630	0.543	1.910	2.679	0.496	13.06
859	0.547	0.402	1.868	2.419	0.489	18.45

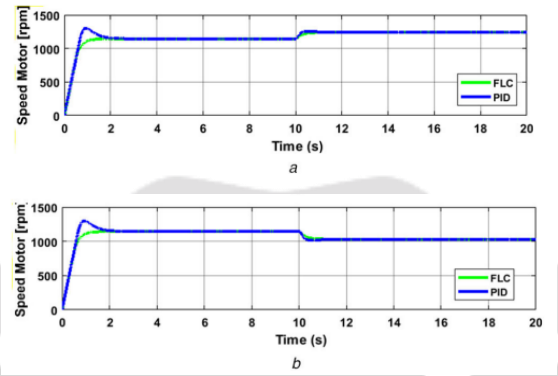

Fig. 17 Speed response comparison for PID and FLC (a), (b) IM response to speed variations ± 100 rpm during 10 s of rated load

7 Conclusion

IM may use more power than necessary when it is operating at a lower than maximum load level. Heat is the result of this extra power. The FLC can be used to regulate the amplitude of the beginning current and during this period, more electricity can be saved. The error of speed and error change, which are utilised in the outer loop to create an equivalent controller term, are the inputs of the fuzzy controller. In this paper, a 50 horsepower IM-driven EV was the subject of a simulation investigation. A variety of performance metrics, including peak overshoot, steady-state error, rising time, and settling time, are tested. The findings demonstrated that there are less loss components (smaller amplitude) with the same order components in the phase current of the recommended system. The proposed FLC scheme's simulation results demonstrated excellent stability and superior performance over the traditional PID controller in peak overshoot, peak rising time, and settling time.

8 References

[1] Sato, E.: 'Permanent magnet synchronous motor drives for hybrid electric vehicles', IEEJ Trans. Electra. Electron. Eng., 2007, 2, (2), pp. 162–168

[2] Agency, I.E.: 'Global EV outlook 2016: beyond one million electric cars' (OECD Publishing)

[3] Sayed, K.: 'Zero-voltage soft-switching DC-DC converter-based charger for LV battery in hybrid electric vehicles', IET Power Electron., 2019, 12, (13), pp. 3389–3396

[4] Gomez, J.C., Morcos, M.M.: 'Impact of EV battery chargers on the power quality of distribution systems', IEEE Power Eng. Rev., 2002, 22, (10), pp. 63–63

[5] Stephan, C.H., Sullivan, J.: 'Environmental and energy implications of plug-in hybrid-electric vehicles', Environ. Sci. Technol., 2008, 42, (4), pp. 1185– 1190

[6] Amatani, S., Fukushima, Y., Morita, H.: 'A linear programming based heuristic algorithm for charge and discharge scheduling of electric vehicles in a building energy management system', Omega, 2017, 67, pp. 115–122

[7] Trove, J.P.F., Roux, M.-A., Menard, E., et al.: 'Energy and power-split management of dual energy storage system for a three-wheel electric vehicle', IEEE Trans. Veh. Technol., 2017, 66, (7), pp. 5540–5550

[8] Buyukdegirmenci, V.T., Bazzi, A.M., Krein, P.T.: 'Evaluation of induction and permanent-magnet synchronous machines using drive-cycle energy and loss minimization in traction applications', IEEE Trans. Ind. Appl., 2014, 50, (1), pp. 395–403

[9] Sargonids, A.G., Beni Akar, M.E., Kladis, A.G.: 'Fast adaptive evolutionary PM traction motor optimization based on electric vehicle drive cycle', IEEE Trans. Veh. Technol., 2016, 66, (7), pp. 5762–5774

[10] Wang, Q., Niu, S., Luo, X.: 'A novel hybrid dual-PM machine excited by AC with DC bias for electric vehicle propulsion', IEEE Trans. Ind. Electron., 2017, 64, (9), pp. 6908–6919

[11] Bouvardia, S., Daim, S., Matia, A.: 'Sensor fault detection and isolation based on artificial neural networks and fuzzy logic applicated on induction motor for electrical vehicle', Int. J. Power Electron. Drive Syst., 2017, 8, (2), pp. 601–611

[12] Varghese, S.T., Rajagopal, K.R.: 'Economic and efficient induction motor controller for electric vehicle using improved scalar algorithm'. IEEE 1st Int. Conf. on Power Electronics, Intelligent Control and Energy Systems (ICPEICES), Delhi, 2016, pp. 1–7

[13] Ulu, C., Korman, O., Komungos, G.: 'Electromagnetic and thermal analysis/ design of an induction motor for electric vehicles. The 8th Int. Conf. on Mechanical and Aerospace Engineering (ICMAE), Prague, 2017, pp. 6–10

[14] Couchette, A., Abbou, A., Akharas, M., et al.: 'Sensor less direct torque control of induction motor using fuzzy logic controller applied to electric vehicle'. Int. Renewable and Sustainable Energy Conf. (IRSEC), Outrate, 2014, pp. 366–372

[15] Makrygiorgou, J.J., Alexandridis, A.T.: 'Induction machine driven electric vehicles based on fuzzy logic controllers. The 42nd Annual Conf. of the IEEE Industrial Electronics Society, Florence, 2016, pp. 184–189

[16] Li, H., Klontz, K.W.: 'Rotor design to reduce secondary winding harmonic loss for induction motor in hybrid electric vehicle application'. IEEE Energy Conversion Congress and Exposition (ECCE), Milwaukee, WI, 2016, pp. 1–6

[17] Kumar, R., Das, S., Chattopadhyay, A.K.: 'Comparative assessment of two different model reference adaptive system schemes for speed-sensor less control of induction motor drives', IET Electra. Power Appl., 2016, 10, (2), pp. 141–154

[18] Saleeb, H., Sayed, K., Kassem, A., et al.: 'Power management strategy for battery electric vehicles', IET Electra. Syst. Transp., 2019, 9, (2), pp. 65–74

[19] Das, S., Pal, A., Manohar, M.: 'Adaptive quadratic interpolation for loss minimization of direct torque-controlled induction motor driven electric vehicle'. IEEE 15th Int. Conf. on Industrial Informatics (INDIN), Emden, 2017, pp. 641–646

[20] Sayed, K., Abo-Khalil, A.G., Alghamdi, A.S.: 'Optimum resilient operation and control dc microgrid based electric vehicles charging station powered by renewable energy sources', Energies, 2019, 12, (22), p. 4240

[21] Sayed, K., El-Zohra, E., Naguib, F., et al.: 'Performance evaluations of interleaved ZCS boost DC-DC converters using quasi-resonant switch blocks for PV interface', IOSR J. elector. Electron. Eng., (IOSR-JEEE), 2015, 10, (4), pp. 105–113

[22] Sayed, K., Gabbar, H.A.: 'Electric vehicle to power grid integration using three-phase three-level AC/DC converter and PI-fuzzy controller', Energies, 2016, 9, p. 532

[23] Jasim, B.H., Dakhil, A.M.: 'New PI and PID tuning rules using simple analytical procedure'. The Second Scientific Engineering Conf., Mousie, Iraq, 2014

[24] Lin, W.-S., Huang, C.-L., Chuang, M.-K.: 'Hierarchical fuzzy control for autonomous navigation of wheeled robots', IEE Proc., Control Theory Appl., 2005, 152, (5), pp. 598–606